Heat Transfer from an Inflow-Type Swirling Turbulent Impinging Jet*

Koichi ICHIMIYA** and Koji TSUKAMOTO***

Heat transfer characteristics of a circular turbulent impinging jet with a swirl were experimentally examined using air as a working fluid. A swirl was produced by inserting air from two exits on the side surface of a circular nozzle. The flow was visualized by a smoke-inducing method. Impingement surface temperature was measured using thermosensitive liquid crystal by transforming from color to temperature. Local heat transfer has two peaks due to the inserting angle. The swirl enhanced the impingement heat transfer, which was arranged by the ratio of circumferential momentum and axial momentum, within the present conditions.

Key Words: Impinging Jet, Swirl, Heat Transfer, Thermosensitive Liquid Crystal, Flow Visualization

1. Introduction

Impinging jets have been used in a variety of applications such as cooling of hot steel plates, cooling of turbine blades, drying of textiles and cooling of electronic equipment[1]. Jet impingement is an effective method of localized heating, cooling and drying. There are many factors which affect impingement heat and mass transfer[2], one of which is the flow situation at the nozzle exit. The impinging flow and turbulent heat transfer of an inclined circular jet within a channel with confining walls were examined experimentally[3]. The local Nusselt number showed the characteristic peak shift in the minor flow region and the plateau in the major flow region on the impingement surface. The behavior of turbulent intensity and acceleration near the surface corresponded to the local heat transfer. The effect of the nozzle shape was also considered using an annular jet[4]. Heat transfer characteristics were denoted by dividing into two regions, the minor flow and the major flow bounded by the position of the peak Nusselt number. The radial Nusselt number was expressed by the function of the radial distance from the center in the minor flow region and by the diameter ratio and the space between nozzle and impingement surface in the major flow region. The effect of buoyancy force was examined numerically and experimentally for a laminar impinging jet[5]. After impingement the heat transfer and flow were classified into three regions, a two-dimensional forced convection region, a three-dimensional mixed convection region and a three-dimensional natural convection region. A recirculating flow on an impingement surface moves downstream with increase of Reynolds number and the space. Streak lines appear in the mixed convection region. The heat transfer of impinging jets from multi-nozzles (three slot nozzles) was examined experimentally[6]. In the laminar jet, the heat transfer increases locally, owing to the flow of the second nozzle. In the turbulent jet, three peaks of the local Nusselt number can be found at the stagnation point of the center nozzle, and the downstream region of the second nozzle. The position of the third peak approaches the second nozzle with the decrease in space. These studies have been confined to non-swirling flows. The application of swirl can markedly affect the flow characteristics of a jet. Ward et al.[7] studied the heat and mass transfer associated with orthogonal impingement of single, swirling, air jets onto a flat surface. The effect of imparting swirl to the jet is to bring about decrease in the heat transfer rate as the swirl number is increased. This is associated with the low velocity core of the swirling jet. Huang et al.[8] estimated numerically the heat transfer under a laminar swirling impinging jet. Addition of swirl was found to enhance spreading at

* Received 17th February, 2006 (No. 06-4037)

** Interdisciplinary Graduate School of Medicine and Engineering, Mechanical Systems Engineering Division, University of Yamanashi, Takeda-4, Kofu, Yamanashi 400–8511, Japan. E-mail: ichimiya@yamanashi.ac.jp

*** Graduate Student of Mechanical Systems Engineering, University of Yamanashi, Takeda-4, Kofu, Yamanashi 400–8511, Japan

a rate dependent on both the swirl number and inlet swirl velocity. A large swirl number generated a toroidal recirculation zone which acts as an insulator and depresses the heat transfer. Wen et al.[9] investigated experimentally the heat transfer of round jets with/without swirling inserts. They showed that the Nusselt number at the stagnation point increases for the case of a round jet with different inserts (longitudinal swirling-strip and crossed swirling-strip) because of flow mixing, formation of vortices on the impingement surface and entrainment of ambient air.

In the present study, the turbulent heat transfer characteristics of an inflow-type swirling impinging jet within confined walls were examined experimentally using thermosensitive liquid crystal for various inserting angles in a comparatively narrow space.

Nomenclature

D : nozzle diameter, m, mm
G_m : axial flux of axial momentum
G_θ : axial flux of angular momentum
h : space between nozzle and impingement surface, mm
Nu : local Nusselt number [refer to Eq. (3)]
Nu_m : mean Nusselt number
Q_m : axial flow rate, m^3/min
$2Qr$: inserting flow rate, m^3/min
q_{net} : net heat flux, W/m^2
q_c : corrected heat flux, W/m^2
r : distance from the nozzle center, mm
Re : Reynolds number at nozzle exit
(r,g,b) : relative light brightness of (Red, Green, Blue)
Sw : Swirl number, G_θ/G_m
Ti : fluid temperature at nozzle exit, °C, K
Tw : impingement surface temperature, °C, K
α : local heat transfer coefficient, W/m^2K
λ : thermal conductivity of fluid, W/mK
θ : inserting angle, °

2. Experimental Apparatus and Procedure

Figure 1 shows a schematic diagram of the experimental apparatus. The apparatus is composed of the flow delivery passage, the heated section including the impingement surface and the temperature measuring system. After the air is compressed in a blower, it is divided into three flow passages. One is an axial air supply and the other two are an angular air supply connected to the side surface of a circular nozzle. The inner diameter of the main nozzle is $D = 30$ mm. The upper wall, set at the same level of the nozzle, is made of acrylic resin and is thermally insulated. The impingement section is composed of an transparent acrylic plate, a thermosensitive liquid crystal sheet and a stainless steel foil. These are closely connected by binding tapes with 99% transparency. The foil is heated electrically. The impingement surface temperature is measured by transforming the color intensity of the thermosensitive liquid crystal sheet to the corresponding temperature. The back side of the impingement section is illuminated by four halogen lamps equipped with infrared radiation absorption filters to prevent radiative heating of the thermosensitive liquid crystal. The color image is converted into an electrical signal by a CCD camera.

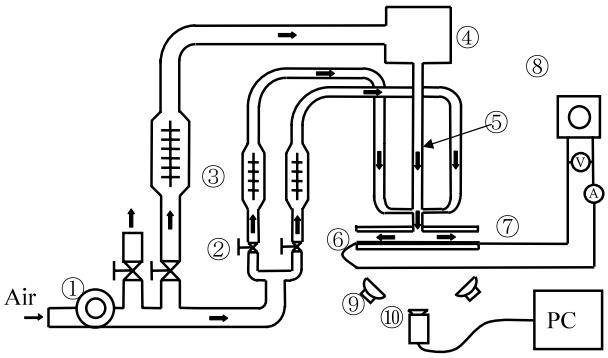

① Blower ② Valve ③ Flow Meter ④ Mixing Chamber
⑤ Nozzle ⑥ Stainless Steel Foil ⑦ Liquid Crystal
⑧ Slide Regulator ⑨ Halogen Lamp ⑩ C.C.D. Camera

Fig. 1 Experimental apparatus

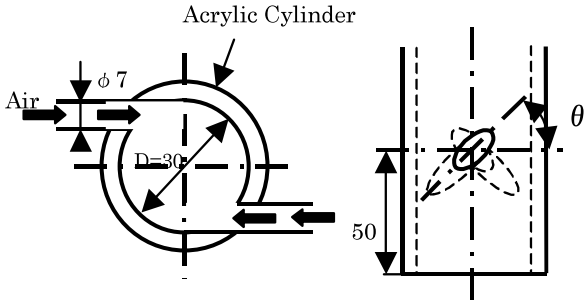

Fig. 2 Nozzle

Figure 2 shows two inserting nozzles on the side surface of the main nozzle. The inner diameter of the inserting nozzle is $d = 7$ mm. The inserting angle is θ. The distance from the end of the main nozzle to the inserting nozzle is 50 mm.

The relationship between light brightness of the thermosensitive liquid crystal and temperature was calibrated in advance[10]. Scattered reflected light from the thermosensitive liquid crystal at a given temperature was divided into three main color components (Red, Green and Blue). The temperature, T, was estimated by a second-order regression equation including the relative light brightness (r, g, b) defined by the ratio of each light brightness to total light brightness.

$$T = \xi \cdot r + \zeta \cdot g + \gamma \cdot r^2 + \delta \cdot g^2 + \varepsilon \cdot rg + \phi \qquad (1)$$

where T is expressed as functions of two relative light brightness levels because $(r + g + b)$ is 1. In the present experiment, the constant values of the equation are ξ =

131.477 3, $\zeta = -435.908$, $\gamma = -166.752$, $\delta = 432.344$, $\varepsilon = 96.339\,87$ and $\phi = 380.074\,3$. The temperature was measured in the range of 32 ~ 41°C, and the accuracy was within 0.3°C. The colors were brown, orange, yellow, green and blue, from low to high temperature.

The local heat transfer coefficient, α and local Nusselt number, Nu, were calculated by the following equations using net heat flux, q_{net},

$$\alpha = q_{\text{net}}/(T_w - T_{\text{in}}) \tag{2}$$

$$Nu = \alpha D/\lambda \tag{3}$$

where T_{in} is the air temperature at the nozzle exit and λ is the thermal conductivity. Net heat flux q_{net} was calculated as the following equation,

$$q_{\text{net}} = q_{\text{unif}} + q_c \tag{4}$$

where q_{unif} is the uniform heat flux by Joule heating and q_c is the corrected heat flux obtained by solving a three-dimensional thermal conduction equation using the detailed temperature distribution in Fig. 4 (b).

In addition, the average Nusselt number was evaluated by averaging the local Nusselt number within dimensionless distance $R(= r/D) = 1.5$ square, as one example.

Swirl generation by two inflows was visualized by a smoke inducing method.

Experiments were carried out in the following conditions to evaluate only the effect of swirl: the Reynolds number at nozzle exit $Re = 11\,500$, the inserting angle $\theta = 0 \sim 60°$, the inserting flow rate $2Qr = 80 \times 10^{-3}$ m^3/min, the axial flow rate $Q_m = 1.814 \times 10^{-1}$ m^3/min and the space between nozzle and impingement surface $h = 10$, 15 and 20 mm.

3. Results and Discussion

In the first stage, Fig. 3 (a) and (b) shows the flow visualization at the inserting nozzle for $\theta = 0°$ and 30°. Swirl was generated by two inflows from two inserting nozzles along the side surface. The inserting angles mean the degree of swirl generation. Swirl construction was not enough in a large inserting angle, but inflow was supplied tangentially in $\theta = 0°$. Main flow and inflow were mixed on the impingement surface.

In the next stage, Fig. 4 (a) – (d) shows the local heat transfer for $h/D = 0.33$ and $\theta = 30°$. Figure 4 (a) shows the color distribution on the impingement surface. Figure 4 (b) indicates the isothermal lines corresponding to Fig. 4 (a). Each thermal line is denoted by color. Two low temperature regions, where the front edges of a swirl impinged, are found on the impingement surface. In these regions, isothermal lines are closed. The yellow-green area presents the high heat flux region because of the high temperature gradient. Figure 4 (c) shows the corrected heat flux. The positive and negative values in each heat flux mean "inflow" to a pixel and "outflow" from a pixel, respectively. Figure 4 (d) shows two-dimensional Nusselt number distribution including the net heat flux. The two peaks of local Nusselt number can be found and the effective area due to a swirl expands to about 3 times in diameter.

Figure 5 (a) – (d) shows the Nusselt number distribution for various inserting angles at $h = 10$ mm. When the edges of the swirl impinged the surface, the local heat transfer was improved and the area was indicated by the color red. The region is larger for $\theta = 0°$ and 60°. In the case of $\theta = 0°$, the swirl expands in the main nozzle. However, in the case of $\theta = 60°$, two inflows impinged with insufficient swirl. Inserting angle $\theta = 90°$ means without swirl. The local Nusselt number takes two peaks in annular form for a turbulent jet[11].

Figure 6 presents the average Nusselt number for the ratio of the circumferential momentum and the axial momentum, Sw. The absolute value of the average Nusselt number is higher for narrow space. This behavior is same as that without swirl. It is not clear why Num peaks at $Sw = 0.78$. We should experiment for various conditions.

Figure 7 shows relationship between the ratio of the Nusselt number with and without swirl and the momentum ratio Sw to express the degree of heat transfer improve-

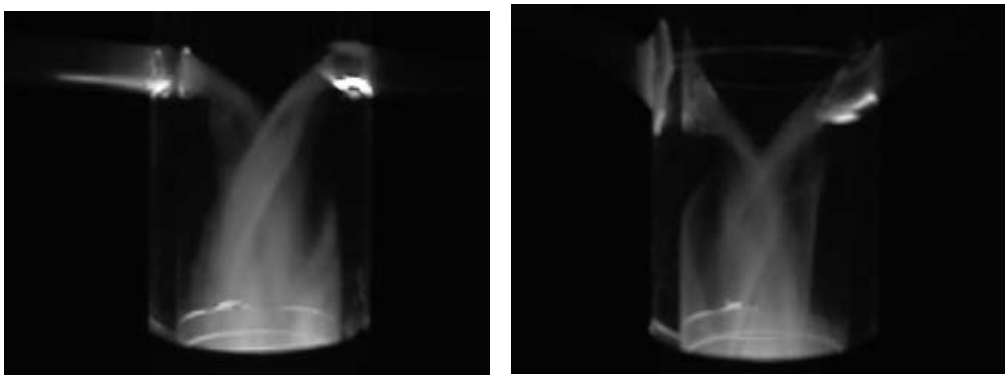

(a) $\theta = 0°$ (b) $\theta = 30°$

Fig. 3 Swirl visualization

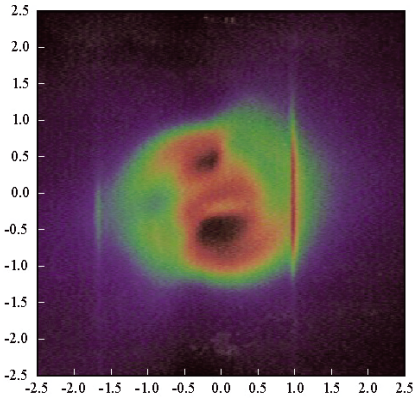

(a) Color distribution

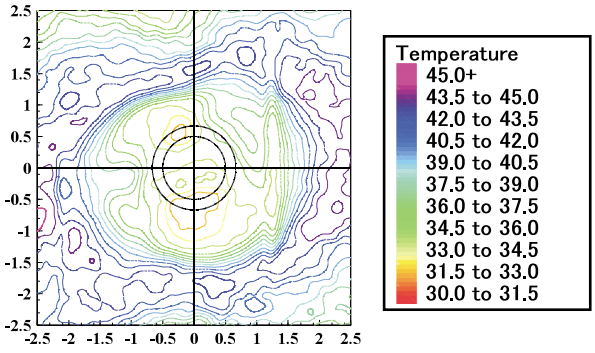

(b) Isothermal lines T [°C]

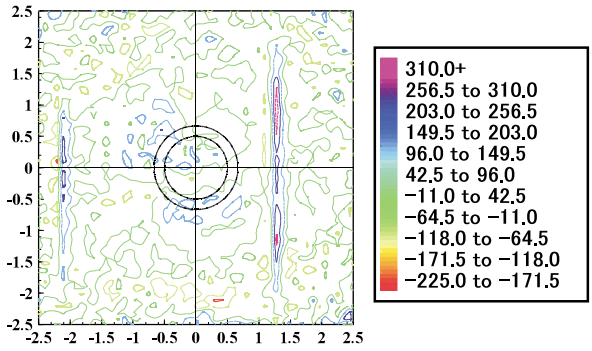

(c) Corrected heat flux q_c [W/m^2]

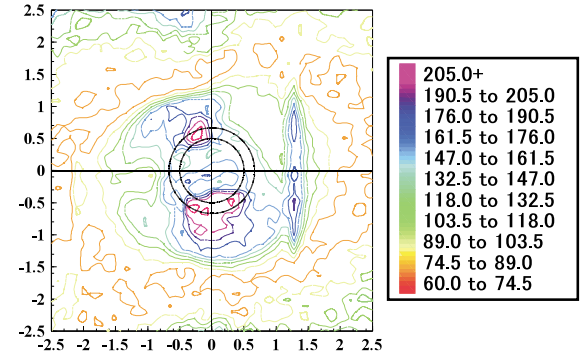

(d) Local Nusselt number

Fig. 4 Heat transfer situation ($Re = 11\,500$, $h/d = 0.33$, $\theta = 30°$)

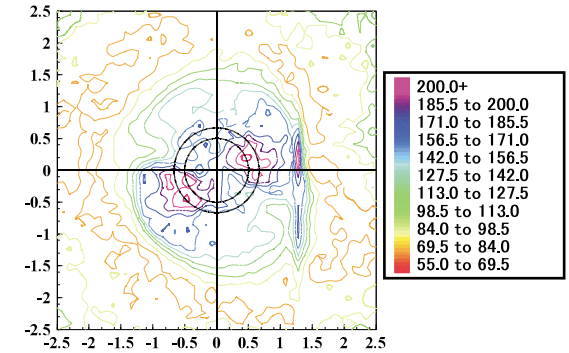

(a) $\theta = 0°$

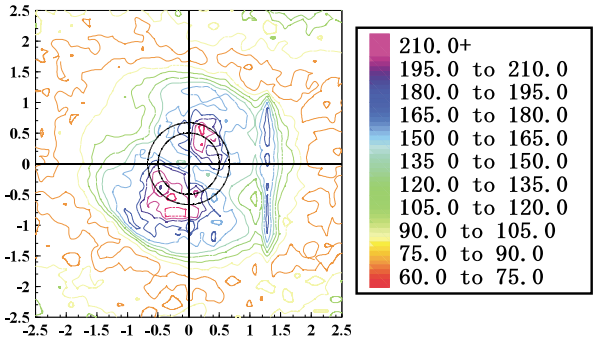

(b) $\theta = 45°$

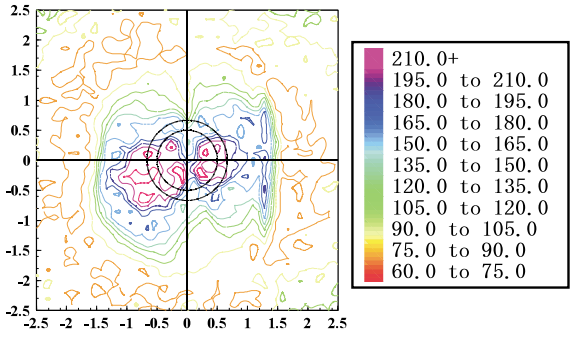

(c) $\theta = 60°$

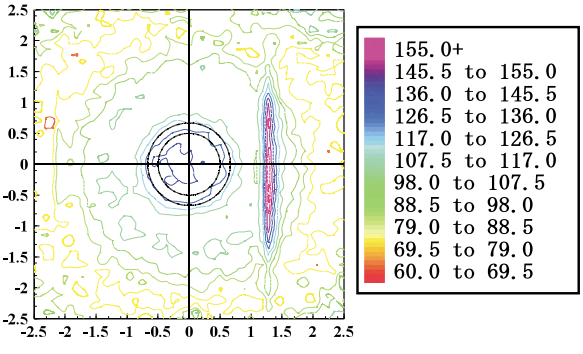

(d) Without swirl

Fig. 5 Local Nusselt number for various inserting angles ($Re = 11\,500$, $h/D = 0.33$)

ment. Heat transfer is enhanced within the present conditions because the value is higher than 1.0. The swirl effect for the heat transfer is higher for a wide space. According to the behavior, results show that the peak of Nusselt

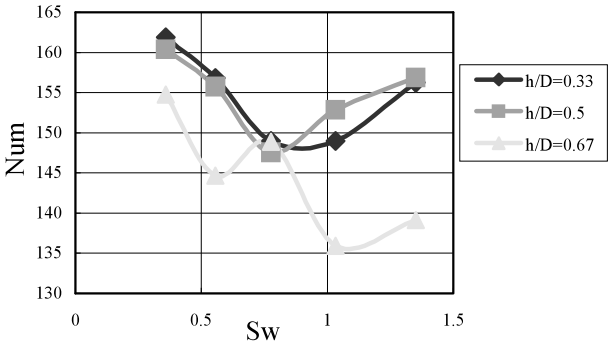

Fig. 6 Average Nusselt number ($Re = 11\,500$)

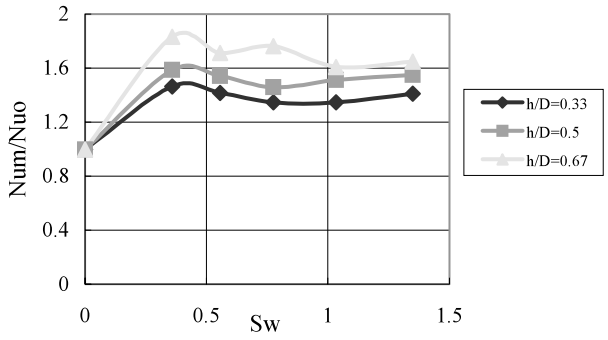

Fig. 7 Nusselt number Num/Nuo ($Re = 11\,500$)

number ratio exists and the ratio tends to decrease as Sw increases.

4. Conclusions

The heat transfer of a circular air jet with a swirl was investigated experimentally at a constant distance from the inserting nozzle to the main nozzle exit for various inserting angles. The local temperature on the impingement surface was obtained in two-dimensional form using a thermosensitive liquid crystal. Various inserting angles mean the degree of swirl generation. The local Nusselt number was improved by flow mixing within the present conditions. The swirl effect was remarkable in higher jet spacing and brought about the peak heat transfer enhancement at a certain momentum ratio, but decreased with the increase of the momentum ratio.

References

(1) Martin, H., Heat and Mass Transfer between Impinging Gas Jets and Solid Surface, Edited by Hartnett, J.P. and Irvine, T.F., Advances in Heat Transfer, Vol.13 (1977), Academic Press, New York.

(2) Viskanta, R., Heat Transfer to Impinging Isothermal Gas and Flame Jets, Experimental Thermal and Fluid Science, Vol.6 (1993), pp.111–134.

(3) Ichimiya, K., Heat Transfer and Flow Characteristics of an Oblique Turbulent Impinging Jet within Confined Walls, Transactions of the ASME, Ser.(C), Journal of Heat Transfer, Vol.117 (1995), pp.316–322.

(4) Ichimiya, K., Heat Transfer Characteristics of an Annular Turbulent Impinging Jet with a Confined Wall Measured by Thermosensitive Liquid Crystal, Heat and Mass Transfer, Vol.39 (2003), pp.545–551.

(5) Ichimiya, K. and Yamada, Y., Three-Dimensional Heat Transfer of a Confined Circular Impinging Jet with Buoyancy Effects, Transactions of the ASME, Ser.(C), Journal of Heat Transfer, Vol.125 (2003), pp.250–256.

(6) Ichimiya, K. and Hosaka, N., Experimental Study of Heat Transfer Characteristics due to Confined Impinging Two-Dimensional Jets, Experimental Thermal and Fluid Science, Vol.5 (1992), pp.803–807.

(7) Ward, J. and Mahmood, M., Heat Transfer from a Turbulent, Swirling, Impinging Jet, Proceedings of the Seventh International Heat Transfer Conference (Munchen), (1982), pp.401–408.

(8) Huang, B., Douglas, W.J.M. and Mujumdar, A.S., Heat Transfer under a Laminar Swirling Impinging Jet—A Numerical Study, Proceedings of the Sixth International Heat Transfer Conference (Toronto), (1978), pp.311–316.

(9) Wen, M.Y. and Jang, K.J., An Experiment Cooling on a Flat Surface by Using Circular Jet with Longitudinal Swirling Strips, International Journal of Heat and Mass Transfer, Vol.46 (2003), pp.4657–4667.

(10) Akino, N., Kunugi, T., Ueda, M. and Kurosawa, A., A Study on Thermo-Camera Using Liquid Crystal (Method of Multiple Regression between Color and Temperature), Trans. Jpn. Soc. Mech. Eng., (in Japanese), Vol.54, No.506, B (1988), pp.2661–2668.

(11) Ichimiya, K. and Nakamura, Y., Heat Transfer of a Single Circular Impinging Jet Considered on Heat Conduction in a Heated Plate, Trans. Jpn. Soc. Mech. Eng., (in Japanese), Vol.58, No.550, B (1992), pp.2031–2035.